Inorg. Chem. **2005**, *44*, 2318–2325

Behavior of Tri(*n*-butyl)ammonium Bis[citrato(3–)-O^1,O^3,O^6]silicate in Aqueous Solution: Analysis of a Sol–Gel Process by Small-Angle Neutron Scattering

Oliver Seiler,[†] Christian Burschka,[†] Dietmar Schwahn,[‡] and Reinhold Tacke*,[†]

Institut für Anorganische Chemie, Universität Würzburg, Am Hubland, D-97074 Würzburg, Germany, and Institut für Festkörperforschung, Forschungszentrum Jülich GmbH, D-52425 Jülich, Germany

Received September 7, 2004

The racemic hexacoordinate silicon(IV) complex tri(*n*-butyl)ammonium bis[citrato(3–)-O^1,O^3,O^6]silicate (**1**) was synthesized by treatment of $Si(OMe)_4$ with 2 molar equiv of citric acid and 2 molar equiv of $N(n\text{-}Bu)_3$. The corresponding germanium analogue, tri(*n*-butyl)ammonium bis[citrato(3–)-O^1,O^3,O^6]germanate (**5**; structurally characterized by single-crystal X-ray diffraction), was obtained analogously, starting from $Ge(OMe)_4$. Upon dissolution in water, the λ^6*Si*-silicate dianion of **1** hydrolyzes spontaneously (formation of $Si(OH)_4$ and citric acid), whereas the λ^6*Ge*-germanate dianion of **5** was found to be stable in water. Aqueous "solutions" of **1**, with concentrations that are significantly higher than the saturation concentration of $Si(OH)_4$, look absolutely clear over a period of several weeks; however, in reality, these solutions are sols with very small particles that slowly grow with time and finally form a gel that precipitates. This sol–gel process was monitored by small-angle neutron scattering (SANS). For reasons of comparison, an aqueous solution of the hydrolytically stable germanium compound **5** was also studied by the SANS technique.

Introduction

In context with our studies on higher-coordinate silicon(IV) complexes and their potential role in silicon biochemistry,[1−7] we have reported on the synthesis and structural characterization of racemic tri(*n*-butyl)ammonium bis[(citrato(3−)-O^1,O^3,O^6]silicate (**1**).[3] Most recently, we have succeeded in synthesizing the related compounds **2**·2MeOH (*meso*-configuration) and **3**·1.73MeOH (racemic),[7] which contain a bis[citrato(3−)-O^1,O^3,O^6]silicate dianion and a bis[citrato(4−)-O^1,O^3,O^6]silicate tetraanion, respectively (for a recent review dealing with higher-coordinate silicon compounds with SiO_5 and SiO_6 skeletons, see ref 8).

The λ^6*Si*-silicate anions of **1**−**3**, with their two tridentate citrato ligands, are not stable in aqueous solution.[3,7] Upon dissolution of **1**, **2**·2MeOH, and **3**·1.73MeOH in water at 20 °C, spontaneous hydrolysis of the λ^6*Si*-silicate anions occurs to give clear aqueous "solutions" (sols), which undergo gel formation after a period of several weeks. In this context, it is interesting to note that the zwitterionic λ^5*Si*-silicate **4**, with its two bidentate citrato ligands, exists in aqueous solution, and the hydrate **4**·H_2O can even be crystallized from water.[9]

To get more information about the above-mentioned sol−gel process, small-angle neutron scattering (SANS) studies of aqueous solutions of **1** were performed. For reasons of comparison, the germanium analogue **5** (which was expected to be hydrolytically stable; in this context, see refs 1, 4, and 6) was included in these studies. We report here on the synthesis and structural characterization of **5** and SANS studies of aqueous solutions of **1** and **5**.

* To whom correspondence should be addressed. E-mail: r.tacke@mail.uni-wuerzburg.de. Phone: (+49)931-888-5250. Fax: (+49)931-888-4609.
[†] Universität Würzburg.
[‡] Forschungszentrum Jülich.

(1) Tacke, R.; Stewart, A.; Becht, J.; Burschka, C.; Richter, I. *Can. J. Chem.* **2000**, *78*, 1380−1387.
(2) Tacke, R.; Burschka, C.; Richter, I.; Wagner, B.; Willeke, R. *J. Am. Chem. Soc.* **2000**, *122*, 8480−8485.
(3) Tacke, R.; Penka, M.; Popp, F.; Richter, I. *Eur. J. Inorg. Chem.* **2002**, 1025−1028.
(4) Seiler, O.; Burschka, C.; Penka, M.; Tacke, R. *Z. Anorg. Allg. Chem.* **2002**, *628*, 2427−2434.
(5) Richter, I.; Penka, M.; Tacke, R. *Inorg. Chem.* **2002**, *41*, 3950−3955.
(6) Seiler, O.; Burschka, C.; Penka, M.; Tacke, R. *Silicon Chem.* **2002**, *1*, 355−365.
(7) Tacke, R.; Bertermann, R.; Burschka, C.; Dragota, S. *Z. Anorg. Allg. Chem.* **2004**, *630*, 2006−2012.
(8) Tacke, R.; Seiler, O. In *Silicon Chemistry: From the Atom to Extended Systems*; Jutzi, P., Schubert, U., Eds.; Wiley-VCH: Weinheim, Germany, 2003; pp 324−337.
(9) Mühleisen, M.; Tacke, R. *Chem. Ber.* **1994**, *127*, 1615−1617.

10.1021/ic048748w CCC: $30.25
Published on Web 03/05/2005

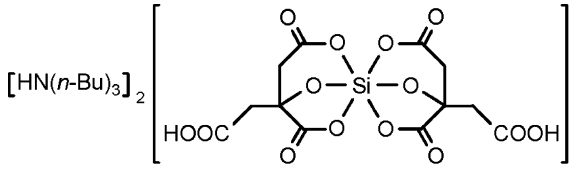

1

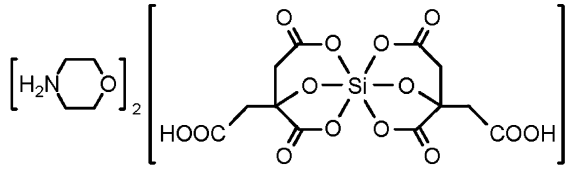

2

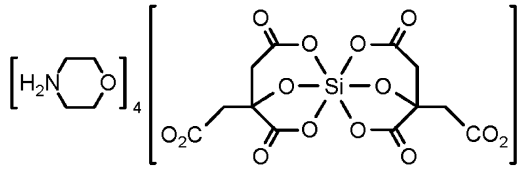

3

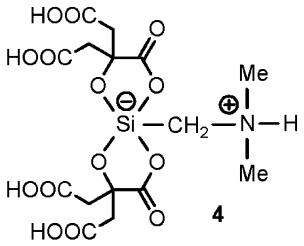

4

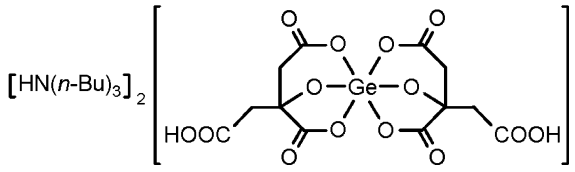

5

Results and Discussion

Syntheses. The racemic hexacoordinate silicon compound **1** was synthesized according to ref 3, starting from tetramethoxysilane. The racemic hexacoordinate germanium analogue, tri(*n*-butyl)ammonium bis[citrato(3−)-O^1,O^3,O^6]-germanate (**5**), was obtained analogously by treatment of tetramethoxygermane with 2 molar equiv of citric acid and 2 molar equiv of tri(*n*-butyl)amine in tetrahydrofuran and was isolated, after recrystallization from ethanol, in 72% yield as a colorless crystalline solid (Scheme 1). The identity of **5** was established by elemental analysis (C, H, N), solution NMR studies (^{1}H, ^{13}C), and single-crystal X-ray diffraction (for the synthesis and crystal structure analysis of a related ammonium bis[methylcitrato(3−)-O^1,O^3,O^6]germanate, see ref 10).

(10) Chiang, H.-C.; Yang, K.-C.; Ueng, C.-H. *J. Chin. Chem. Soc.* **1994**, *41*, 59−63.

Scheme 1

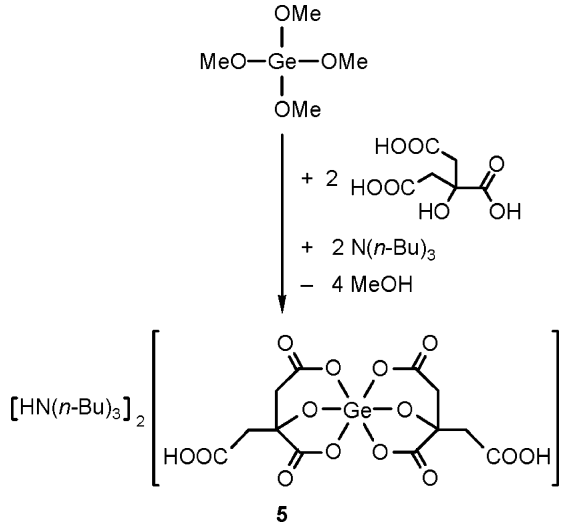

5

Table 1. Crystal Data and Experimental Parameters for the Crystal Structure Analysis of **5**

empirical formula	$C_{36}H_{66}GeN_2O_{14}$
formula mass, g mol^{-1}	823.50
collection *T*, K	173(2)
λ(Mo Kα), Å	0.71073
cryst syst	monoclinic
space group (No.)	$P2_1/n$ (No. 14)
a, Å	10.7426(9)
b, Å	15.6919(8)
c, Å	25.024(2)
β, deg	96.796(10)
V, Å^3	4188.7(5)
Z	4
D (calcd), g cm^{-3}	1.306
μ, mm^{-1}	0.795
F(000)	1760
cryst dimensions, mm	0.4 × 0.3 × 0.3
2θ range, deg	5.04−53.90
index ranges	$-13 \le h \le 13$, $-18 \le k \le 19$, $-31 \le l \le 31$
no. collected reflns	39608
no. independent reflns	8886
R_{int}	0.0363
no. reflns used	8886
no. params	525
no. restraints	5
S^a	1.037
weight params a/b^b	0.0553/0.0000
R1^c [$I > 2\sigma(I)$]	0.0306
wR2^d (all data)	0.0811
max/min residual electron density, e Å^{-3}	+0.460/−0.631

^{a} $S = \{\sum[w(F_o^2 - F_c^2)^2]/(n-p)\}^{0.5}$; n = no. of reflections; p = no. of parameters. ^{b} $w^{-1} = \sigma^2(F_o^2) + (aP)^2 + bP$, with $P = [\max(F_o^2,0) + 2F_c^2]/3$. ^{c} $R1 = \sum||F_o| - |F_c||/\sum|F_o|$. ^{d} $wR2 = \{\sum[w(F_o^2 - F_c^2)^2]/\sum[w(F_o^2)^2]\}^{0.5}$.

Crystal Structure Analysis. The crystal data and the experimental parameters used for the crystal structure analysis of **5** are given in Table 1; selected bond distances and angles are listed in Table 2. The structure of the λ^6*Ge*-germanate dianion in the crystal is shown in Figure 1.

The crystal structures of the Si/Ge analogues **1**[3] and **5** were found to be isotypic. The Ge-coordination polyhedron of **5** represents a distorted octahedron, with O−Ge−O angles in the ranges 86.38(4)−94.43(5)° and 173.21(4)−178.43(4)°. The two tridentate citrato(3−) ligands are coordinated to the germanium(IV) coordination center each with two carboxy-

Table 2. Selected Bond Distances [Å] and Angles [deg] for **5**

Ge−O1	1.8321(10)	Ge−O4	1.8190(10)
Ge−O2	1.9202(11)	Ge−O5	1.9120(11)
Ge−O3	1.9039(11)	Ge−O6	1.9232(10)
O1−Ge−O2	86.38(4)	O2−Ge−O6	89.19(5)
O1−Ge−O3	92.49(5)	O3−Ge−O4	88.85(5)
O1−Ge−O4	178.43(4)	O3−Ge−O5	91.06(5)
O1−Ge−O5	86.89(4)	O3−Ge−O6	175.61(5)
O1−Ge−O6	91.79(5)	O4−Ge−O5	92.28(5)
O2−Ge−O3	90.12(5)	O4−Ge−O6	86.88(4)
O2−Ge−O4	94.43(5)	O5−Ge−O6	90.13(5)
O2−Ge−O5	173.21(4)		

Table 3. Hydrogen-Bonding Geometries for **5**[a]

D−H···A	D−H [Å]	H···A [Å]	D···A [Å]	D−H···A [deg]
N1−H1···O3	0.88(2)[b]	2.53(2)	3.1086(17)	124.1(16)
N1−H1···O8	0.88(2)[b]	1.98(2)	2.8525(18)	169.5(19)
N2−H2···O10	0.83(2)	2.02(2)	2.842(2)	168(2)
O11−H11···O1	0.89(3)	1.76(3)	2.5907(16)	155(2)
O14−H14···O13	0.91(2)	1.73(2)	2.6254(17)	171(2)

[a] Data calculated by using the program PLATON.[11] Since the H2···O5 distance in the crystal structure of **5** is longer than 2.60 Å, the program PLATON does not recognize an intramolecular N2−H2−O5 interaction as observed for the isotypic crystal structure of **1**.[3] [b] O3···H1···O8 = 56.9(5)°.

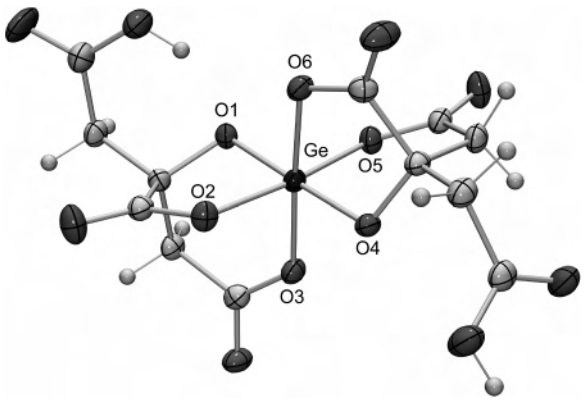

Figure 1. Structure of the λ^6*Ge*-germanate dianion in the crystal of **5** (probability level of displacement ellipsoids 50%).

lato oxygen atoms (O2/O3, O5/O6) and one alcoholato oxygen atom (O1, O4), forming two bicyclic moieties each with a five-, six-, and seven-membered ring. The Ge−O(carboxylato) distances range from 1.9039(10) to 1.9232(10) Å, whereas the Ge−O(alcoholato) distances are in the range 1.8190(10)−1.8321(10) Å.

As expected from the presence of the potential N*H* donor functions of the two ammonium cations and the potential oxygen acceptor atoms of the λ^6*Ge*-germanate dianion, hydrogen bonds are observed in the crystal of **5** (Table 3, Figure 2).[11] Intermolecular bifurcate N1−H1···O3/O8 hydrogen bonds and intermolecular O14−H14···O13 and N2−H2···O10 interactions lead to the formation of centrosymmetric aggregates consisting of two dianions and four cations. In addition, there is an intramolecular O11−H11···O1 hydrogen bond.

(11) The hydrogen-bonding system was analyzed by using the program PLATON: Spek, A. L. *PLATON*; University of Utrecht: Utrecht, The Netherlands, 1998. In this context, see also: Jeffrey, G. A.; Saenger, W. *Hydrogen Bonding in Biological Structures*; Springer-Verlag: Berlin, Germany, 1991; pp 15−24.

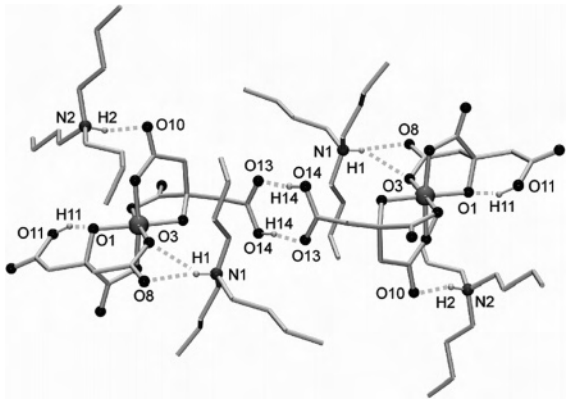

Figure 2. Hydrogen-bonding system in the crystal of **5**. The dashed lines indicate hydrogen bonds that lead to the formation of isolated centrosymmetric aggregates consisting of two anions and four cations. The hydrogen atoms (except O*H* and N*H*) are omitted for clarity, and the carbon atoms are represented as stick models.

NMR Studies and pH Measurements. The ^{1}H and ^{13}C NMR spectra of the germanium compound **5** in CD_3CN and CD_3OD are very similar to those obtained for the silicon analogue **1**.[3,12] However, in contrast to the λ^6*Si*-silicate dianion, the λ^6*Ge*-germanate dianion was found to be hydrolytically stable upon dissolution in water, and compound **5** could even be recrystallized from water. The ^{1}H NMR spectrum of **5** in D_2O (one set of resonance signals) is almost identical with the NMR data for the major species in the solutions of **5** in CD_3CN and CD_3OD. The spontaneous hydrolysis of the λ^6*Si*-silicate dianion in D_2O is reflected by the characteristic resonance signals of free citric acid in the ^{1}H NMR spectrum (δ 2.60 (δ_A) and 2.71 (δ_B), CCH_AH_BC, $^2J_{AB}$ = 15.5 Hz) and by the characteristic resonance signal for monosilicic acid ($Si(OH)_4$) (δ −72.2) in the ^{29}Si NMR spectrum.

To get information about the pH values of the aqueous solution of **1** and **5** that were studied by the SANS technique, pH measurements were performed at 20 °C over a time period of 30 days. For a freshly prepared aqueous solution of the silicon compound **1** (concentration, 48.8 mg mL^{-1} (62.6 mM)), a value of pH 3.7 was measured. For an aqueous solution of the germanium analogue **5** (concentration, 51.6 mg mL^{-1} (62.6 mM)), a value of pH 3.3 was determined. Both solutions did not change their pH value significantly over the time period studied. To adjust a pH value of pH 6.5, solid sodium hydroxide was added to an aqueous solution of **1** in water (concentration, 48.8 mg mL^{-1} (62.6 mM)) at 20 °C. The resulting "solution" continued to remain clear over a period of at least 8 days.

SANS Studies. To get information about the behavior of the silicon compound **1** in aqueous solution (hydrolysis and subsequent sol−gel process), solutions of **1** in methanol and water were studied with the SANS technique. For reasons

(12) As also observed for the silicon analogue **1**,[3] there was one set of very intense resonance signals for the citrato(3−) ligands in the ^{13}C NMR spectrum of **5** that are compatible with the structure of the λ^6*Ge*-germanate dianion. In addition, there were some significantly less intense signals that point to the presence of other species in solution. The ^{13}C NMR data given correspond to the major species in CD_3CN and CD_3OD.

Table 4. Parameters for the SANS Studies

	chemical formula	atomic mass [10^{-21} g]	density [g mL^{-1}]	ρ [10^{10} cm^{-2}]
1	$C_{36}H_{66}N_2O_{14}Si$	1.29	1.256	0.898
5	$C_{36}H_{66}GeN_2O_{14}$	1.37	1.306	0.967
water	D_2O	0.0333	1.1079	6.39
methanol	CD_4O	0.0599	0.89	5.82

Table 5. Parameters Evaluated from the SANS Data[a]

	solvent	R_g [Å]	dΣ/dΩ($Q = 0$) M^{-1} c^{-1} [10^{20} cm^2 g^{-2}]	density [g mL^{-1}]
1	CD_3OD	6.5 ± 0.2	9.4 ± 0.5	1.5 ± 0.1
5	D_2O	4.0 ± 0.2	6.4 ± 0.3	1.97 ± 0.13

[a] M = atomic mass; c = concentration.

of comparison, a solution of the germanium analogue **5** in water was also investigated. To achieve a high scattering contrast, the SANS experiments were performed with solutions of **1** and **5** in the deuterated solvents CD_3OD and D_2O, respectively. The parameters for the SANS studies are summarized in Table 4, and the parameters evaluated from the SANS data are given in Table 5. The results of these studies are shown in Figures 3−8.

The macroscopic scattering cross section dΣ/dΩ(Q) is proportional to the intensity of the scattered neutrons and is given as a function of the scattering vector modulus Q. The unit of dΣ/dΩ is cm^{-1} and represents the scattering per unit volume, while Q is defined as $Q = (4\pi/\lambda)\sin(\delta/2)$, with λ and δ being the neutron wavelength and scattering angle, respectively. The scattered neutrons are described by Beaucage's law, representing a combination of Guinier's and Porod's laws, according to eq 1,

$$\frac{d\Sigma}{d\Omega}(Q) \approx \frac{d\Sigma}{d\Omega}(Q=0)\exp(-R_g^2Q^2/3) + P_\alpha(1/Q^*)^\alpha \quad (1)$$

with $Q^* = Q/[\mathrm{erf}(1.06QR_g/\sqrt{6})]^3$.[13] Guinier's and Porod's laws are valid at low and large Q in comparison with the inverse radius of gyration R_g, and the erf in Q^* takes care that both terms only contribute within their ranges of validity. The parameters derived from eq 1 are dΣ/dΩ($Q = 0$), representing the extrapolated scattering at $Q = 0$, the radius of gyration R_g, the Porod constant P_α, and the exponent α. The scattering at $Q = 0$ is determined according to dΣ/dΩ($Q = 0$) = $\Phi V \Delta\rho^2$ from the domain volume fraction Φ, volume V, and the difference of the scattering length density $\Delta\rho = (\rho_P - \rho_S)$ of the domains and the solvent. The definition of the Porod constant depends on the exponent: generally, one observes $4 > \alpha > 3$ for surface fractals, $3 > \alpha > 1$ for mass fractals, and $\alpha > 4$ for diffuse interfaces. The shape of compact particles is characterized as follows: rods by $\alpha = 1$, disks by $\alpha = 2$, 3D particles by $\alpha = 4$, and porous particles by $\alpha = 3$.[14] The experiments performed in this study will be interpreted in terms of dΣ/dΩ($Q = 0$), R_g, and the exponent α.

Figure 3 shows the results obtained for solutions of **1** in CD_3OD at two different concentrations (48.8 and 97.6 mg mL^{-1}; temperature, 20 °C). The solid lines of the graph represent a fit of eq 1 with $P_\alpha = 0$. The radius of gyration lies between 6.4 and 6.6 Å, and the scattering intensity at $Q = 0$ is proportional to the concentration, indicating the presence of a solution of individual species (ions and/or ion pairs). Figures 4 and 5 show the behavior of aqueous solutions (concentration, 48.8 mg mL^{-1}) at 20 and 50 °C. A continuous increase of scattering intensity by 3 orders of magnitude is observed over a time period of 49 days. During the first 6 h (Figure 4), the particles increase linearly from sizes of about 4.5 Å (radius of gyration) to the original size of the particles determined in CD_3OD. This is consistent with the hydrolysis of the λ^6*Si*-silicate dianion to form monosilicic acid ($Si(OH)_4$) and free citric acid (decrease of molecular size), followed by condensation of the silicic acid (increase of molecular size). A linear increase is also observed for dΣ/dΩ($Q = 0$) (Figure 4b). Assuming a constant volume fraction for **1**, an increase proportional to R_g^3 is expected in contrast to the much weaker increase observed. Thus, it is evident that the λ^6*Si*-silicate dianion is destroyed by hydrolysis, resulting in the formation of appreciably smaller particles (monosilicic acid and citric acid as the primary hydrolysis products). After about 7 h, intensity starts to increase faster in the lower Q regime as depicted in the bottom panel of Figure 4a. This result can be explained by the formation of larger particles presumably generated by condensation of silicic acid. These scattering patterns cannot be analyzed in terms of Guinier's law as the size distribution of the particles is too large.

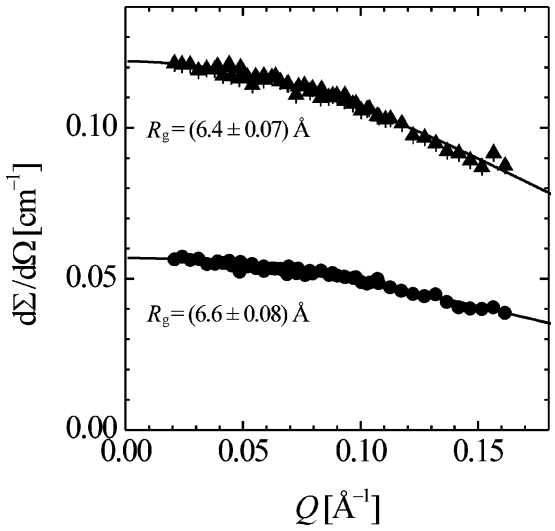

Figure 3. SANS scattering patterns from solutions of **1** in CD_3OD at concentrations of 48.8 mg mL^{-1} (●) and 97.6 mg mL^{-1} (▲) (temperature 20 °C). Compound **1** is characterized by the radius of gyration and the extrapolated scattering at $Q = 0$, which is proportional to the concentration as expected.

Figure 5a shows the scattering patterns representing a time evolution between 19 h and 49 days. Between 19 and 166 h, the sol showed a continuous increase of the scattering intensity, whereas a characteristically different scattering pattern was observed after gel formation (measurement after 49 days). While the scattering of the sol shows Guinier's behavior (first term in eq 1) at small Q, all curves meet on a single curve at large Q. On the other hand, the gel

(13) Beaucage, G. *J. Appl. Crystallogr.* **1996**, *29*, 134−146.
(14) Roe, R.-J. *Methods of X-Ray and Neutron Scattering in Polymer Science*; Oxford University Press: Oxford, U.K., 2000; pp 160−162, 188−193.

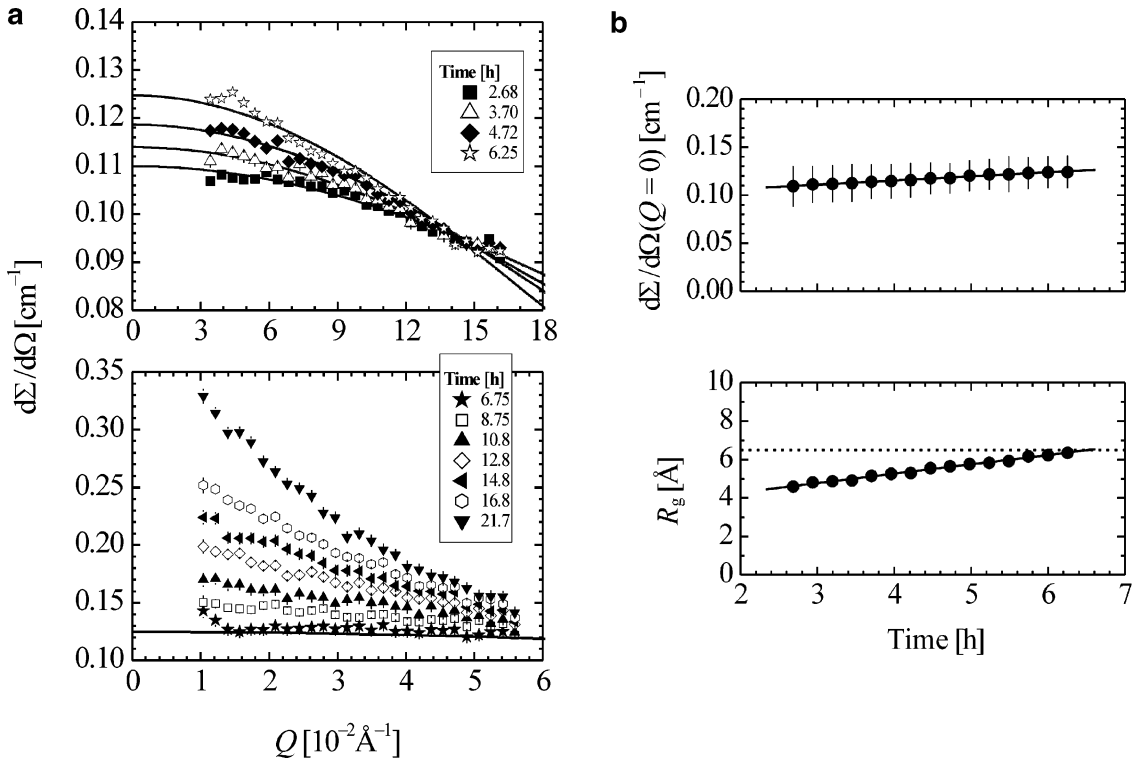

Figure 4. (a) SANS scattering patterns of a solution of **1** in D_2O (concentration, 48.8 mg mL^{-1}) at the beginning of the sol−gel process (temperature, 20 °C). During the first 6 h, the data can be described by Guinier's law as shown by the solid lines (top panel). After 6 h, larger particles become visible as shown in the bottom panel. (b) Plot of the radius of gyration and the intensity at $Q = 0$ as a function of time. The data were obtained by SANS experiments with a solution of **1** in D_2O (concentration, 48.8 mg mL^{-1} at 20 °C. The dashed line represents R_g of **1** as determined for a solution of **1** in CD_3OD (concentration, 48.8 mg mL^{-1}) at 20 °C. In aqueous solution, the particles first decrease by hydrolysis of the λ^6*Si*-silicate dianion and then increase by condensation of silicic acid.

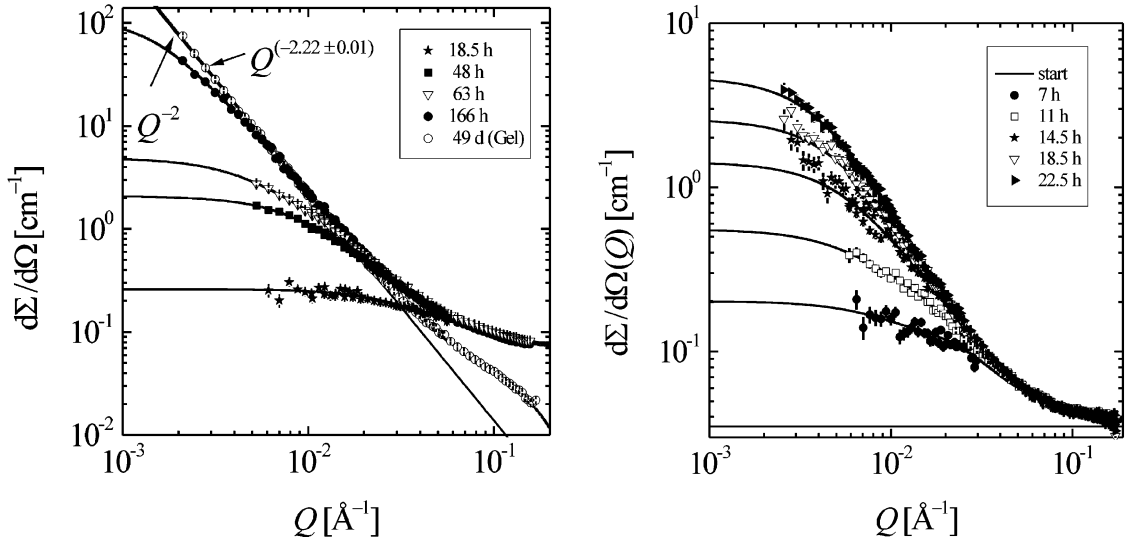

Figure 5. (a) SANS scattering patterns of a solution of **1** in D_2O (concentration, 48.8 mg mL^{-1}) at 20 °C at 18.5 h and beyond. The scattering intensity steadily increases with time and, depending on *Q*, approaches at earlier or later time a borderline. The solid lines represent a fit of Beaucage's model function for mass fractal structures. After 166 h, a Q^{-2} power law is found. (b) SANS scattering patterns of a solution of **1** in D_2O (concentration, 48.8 mg mL^{-1}) at 50 °C at 7 h and beyond.

shows no Guinier regime, and an exponential shape with $\alpha = 2.22 \pm 0.01$ is observed, which is characteristic of mass fractal geometry. In addition, at large *Q* a lower scattering intensity is observed for the gel phase, characterizing the units of the mass fractal. An analysis of this scattering behavior reveals a particle size of the order of 10 ± 5 Å (radius of gyration), with indications of a platelike shape, indicating that the sol−gel transition of the present system is also accompanied by a transition on a microscopic scale. Figure 5b shows the time evolution of a solution of **1** in D_2O at 50 °C in the sol state for a time period of nearly 1 day. The scattering data look very similar to those of the sol phase at 20 °C (Figure 5a).

The scattering patterns of the sol phases in Figure 5 are well described by the scattering law of eq 1 as demonstrated by the solid lines. This scattering law allows a relatively good

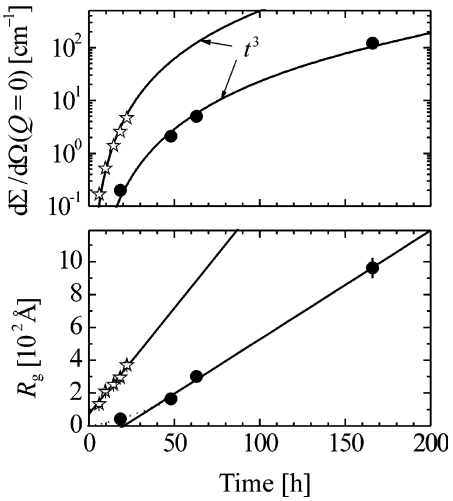

Figure 6. Plots of the radius of gyration and the intensity at $Q = 0$ for solutions of **1** in D_2O (concentration, 48.8 mg mL^{-1}) at 20 °C (●) and 50 °C (☆) as a function of time. The plots were generated from the data given in Figure 5. R_g increases linearly with time, by a factor of 2.7 faster at 50 °C as compared to 20 °C. $d\Sigma/d\Omega(Q = 0)$ increases as a function of time with the third power 20 times faster at 50 °C as compared to 20 °C.

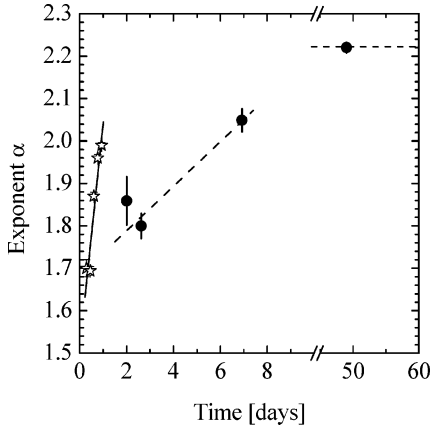

Figure 7. Plot of the exponents of Q as a function of time. The data were obtained by SANS experiments with solutions of **1** in D_2O (concentration, 48.8 mg mL^{-1}) at 20 °C (●) and 50 °C (☆). The observed exponents between 1.7 and 2.3 are characteristic of mass fractal objects. The larger exponents at later time result from a densification of the aggregates.

characterization of fractal objects with an upper and lower characteristic length describing the range of the power law according to $Q^{-\alpha}$. The fit parameters $d\Sigma/d\Omega(Q = 0)$ and the radius of gyration R_g are depicted in Figure 6; the fractal dimensionality α is shown in Figure 7. The radius of gyration gives the upper characteristic size of the fractal objects and can be taken for a correlation length of the domains, while the microscopic length must be smaller than 3 Å as derived from the deviation of the power law above $Q > 0.05$ $Å^{-1}$. It is proposed that the growth process occurs by coagulation of the already existing aggregates. This can be concluded from the following observations: (i) the scattering intensity approaches a kind of master curve as observed in the range $Q > 0.02$ $Å^{-1}$ and (ii) the scattering intensity at $Q = 0$ increases proportional with R_g^3 as seen from the time dependence of R_g and $d\Sigma/d\Omega(Q = 0)$. This means that the volume fraction of the aggregated domains is constant with time; that is, all particles are precipitated within the domains. The Q^{-2} power law observed at 20 °C after 7 days gives a hint of platelike structures. Generally, a densification of the domains can be concluded from the increase of the fractal dimensionality depicted in Figure 7.

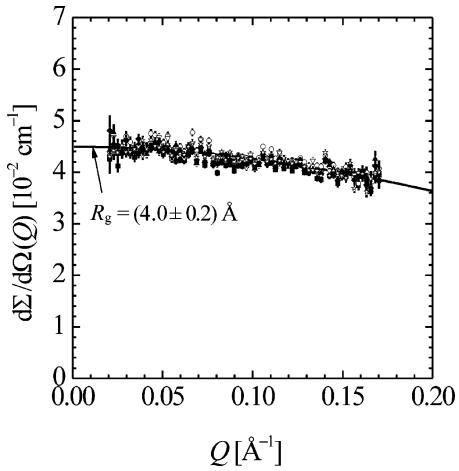

Figure 8. SANS scattering patterns from a solution of **5** in D_2O (concentration, 51.6 mg mL^{-1}) at 40 °C. No change of scattering intensity is observed over a time period of 31 h.

When the sol−gel process is compared at 20 and 50 °C, a lower scattering intensity is found for the experiment at 50 °C in the high Q range (0.04 cm^{-1} (50 °C) versus 0.07 cm^{-1} (20 °C)). This observation gives a hint that the particles at 50 °C degenerate to a smaller size, which is of the order of half of the volume measured at 20 °C. As can be seen from Figure 6, the radius of gyration shows a linear increase (which is faster by a factor of 2.7 at 50 °C) and a corresponding increase of $d\Sigma/d\Omega(Q = 0)$ with power 3, and a 20 times faster growth at 50 °C is observed. Within the sol phase, the exponent α shows an increase with time from 1.7 to nearly 2.1 (Figure 7). These exponents mean that the sol phase, whose size is given by the radius of gyration, is represented by mass fractal geometry, which becomes more compact with time.

Figure 8 collects all scattering data obtained for a solution of **5** in D_2O (concentration, 51.6 mg mL^{-1}) at 40 °C measured over a time period of 31 h. No change of scattering intensity was observed, indicating stability of the λ^6*Ge*-germanate dianion in water. Only the data measured at large Q are depicted, but the corresponding experiments at smaller Q showed no time effect as well.

Conclusions

The ^1H, ^{13}C, and ^{29}Si NMR spectra of solutions of the silicon compound **1** in CD_3CN and CD_3OD are compatible with the existence of the bis[citrato(3−)]silicate dianion in these organic solvents. As shown by ^1H and ^{13}C NMR studies of the germanium analogue **5**, the bis[citrato(3−)]germanate dianion exists in CD_3CN and CD_3OD as well and is even stable in water. However, upon dissolution of the silicon compound **1** in water at 20 °C, the λ^6*Si*-silicate dianion is spontaneously hydrolyzed to give citric acid and monosilicic acid as demonstrated by NMR studies. For a 62.6 mM aqueous solution of **1**, a pH value of 3.7 was measured, which did not change significantly over a period of 30 days. During this time, the aqueous solution looked absolutely clear.

It is interesting to note that the concentration of the resulting monosilicic acid (62.6 mM) is significantly higher than its saturation concentration (ca. 2 mM), and hence, a spontaneous precipitation of silica gel would be expected. Even higher concentrated aqueous "solutions" of **1** (125 mM) looked absolutely clear for a period of at least 10 days, and a 62.6 mM "solution" at pH 6.5 remained clear over a period of at least 8 days as well. However, in reality, these "solutions" are sols with very small particles that slowly grow with time and finally form a gel that precipitates. The SANS technique proved to be a powerful tool to monitor this sol−gel process in detail. In the case of a 62.6 mM aqueous "solution" of **1**, gel formation was observed after a period of 30 days. The chemical nature of the sol particles was not studied, but presumably they are built up by polysilicic acid (formed by condensation of monosilicic acid), which is stabilized by tri(*n*-butyl)ammonium cations and/or citric acid.

As demonstrated recently, fluorescence anisotropy decay is a powerful alternative to scattering techniques for the analysis of silica particle growth in sols.[15−17] When this experimental method is used, it has been shown[18] that glycerol as an organic polyhydroxy compound (as in the case of our tri(*n*-butyl)amine/citric acid system) significantly suppresses the rate of silica particle growth in aqueous systems (in this context, see also ref 19).

In recent years, significant progress has been made in the understanding of silica biomineralization, especially in the case of diatoms[20−24] (for a recent survey of literature dealing with silicon biochemistry, see ref 25). However, despite the many advances in our understanding of biogenic silica precipitation, surprisingly little is known about how silicon is stored in biological systems. Experiments have demonstrated dissolved silicon in the "soluble silicon pool" in diatoms at levels 2 orders of magnitude higher than the saturation concentration of monosilicic acid in water.[26] To explain this phenomenon, it has been postulated that silicon may be stored as silicon(IV) complexes with organic ligands.[27−31] However, the chemical nature of these hypothetical silicon species in the soluble silicon pool is still completely unknown, and the biological relevance of such silicon complexes (especially those with penta- or hexacoordinate silicon atoms) is discussed very controversially. Despite our own (up to now unsuccessful) efforts to verify this hypothesis experimentally,[1−7] we would like to suggest again an alternative (or additional) mechanism for the storage of "dissolved" silicon in biological systems: inspired by the results of the present study and the data reported in refs 18 and 19, silicon storage based on sols is proposed that are built up by aggregates of polysilicic acid, which are stabilized by organic components (in this context, see also ref 26). However, to verify this speculative suggestion, further extensive studies are necessary.

Experimental Section

Chemistry. General Procedures. The syntheses were carried out under dry nitrogen. The organic solvents used were dried and purified according to standard procedures and stored under nitrogen. The melting points were determined with a Büchi Melting Point B-540 apparatus using samples in sealed capillaries. The pH measurements were performed with a Mettler Toledo MP220 pH meter using a Toledo InLab410 electrode. The ^{1}H, ^{13}C, and ^{29}Si solution NMR spectra were recorded at 22 °C on a Bruker DRX-300 NMR spectrometer (^{1}H, 300.1 MHz; ^{13}C, 75.5 MHz; ^{29}Si, 59.6 MHz). CD_3CN, CD_3OD, and D_2O were used as the solvents. Chemical shifts (ppm) were determined relative to internal CHD_2CN (^{1}H, δ 1.93; CD_3CN), internal CHD_2OD (^{1}H, δ 3.30; CD_3OD), internal HDO (^{1}H, δ 4.70; D_2O), internal CD_3CN (^{13}C, δ 1.30; CD_3CN), internal CD_3OD (^{13}C, δ 49.0; CD_3OD), internal TSP (sodium 2,2,3,3-tetradeutero-3-(trimethylsilyl)propanoate) (^{13}C, δ 0; D_2O), or external TMS (^{29}Si, δ 0; CD_3OD, D_2O). Assignment of the ^{13}C NMR data was supported by DEPT 135 experiments.

Racemic Tri(*n*-butyl)ammonium Bis[citrato(3−)-*O*^{1},*O*^{3},*O*^{6}]-silicate (1). This compound was synthesized according to ref 3. ^{1}H NMR (CD_3OD): δ 0.96−1.01 (m, 18 H, CCH_3), 1.34−1.46 (m, 12 H, CCH_2CH_3), 1.62−1.72 (m, 12 H, NCH_2CH_2C), 2.54−2.92 (m, 8 H, $CCH_2C(O)$), 3.12−3.17 (m, 12 H, NCH_2C). ^{13}C NMR (CD_3OD): δ 14.0 (CCH_3), 20.9 (CCH_2CH_3), 26.7 (NCH_2CH_2C), 41.8 ($CCH_2C(O)$), 44.0 ($CCH_2C(O)$), 53.8 (NCH_2C), 74.5 (C_3CO), 169.7 (C═O), 173.4 (C═O), 175.5 (C═O). ^{29}Si NMR (CD_3OD): δ −166.4.

Racemic Tri(*n*-butyl)ammonium Bis[citrato(3−)-*O*^{1},*O*^{3},*O*^{6}]-germanate (5). Tetramethoxygermane (256 mg, 1.30 mmol) was added at 20 °C to a stirred solution of citric acid (500 mg, 2.60 mmol) and tri(*n*-butyl)amine (482 mg, 2.60 mmol) in tetrahydrofuran (10 mL). The reaction mixture was kept undisturbed at 20 °C for 24 h, and the resulting precipitate was isolated by filtration. After recrystallization from ethanol (5 mL; cooling of a boiling solution to room temperature), the product was isolated in 72% yield as a colorless crystalline solid (771 mg, 936 μmol); mp 187

(15) Birch, D. J. S.; Geddes, C. D. *Phys. Rev. E* **2000**, *62*, 2977−2980.
(16) Geddes, C. D.; Karolin, J.; Birch, D. J. S. *J. Fluoresc.* **2002**, *12*, 135−137.
(17) Geddes, C. D. *J. Fluoresc.* **2002**, *12*, 343−367.
(18) Tleugabulova, D.; Duft, A. M.; Zhang, Z.; Chen, Y.; Brook, M. A.; Brennan, J. D. *Langmuir* **2004**, *20*, 5924−5932.
(19) Brook, M. A.; Chen, Y.; Guo, K.; Zhang, Z.; Jin, W.; Deisingh, A.; Cruz-Aguado, J.; Brennan, J. D. *J. Sol.-Gel Sci. Technol.* **2004**, *31*, 343−348.
(20) Tacke, R. *Angew. Chem.* **1999**, *111*, 3197−3200; *Angew. Chem., Int. Ed.* **1999**, *38*, 3015−3018.
(21) Kröger, N.; Sumper, M. In *Biomineralization*; Baeuerlein, E., Ed.; Wiley-VCH: Weinheim, Germany, 2000; pp 151−170.
(22) Hildebrand, M. In *Biomineralization*; Baeuerlein, E., Ed.; Wiley-VCH: Weinheim, Germany, 2000; pp 171−188.
(23) Wetherbee, R.; Crawford, S.; Mulvaney, P. In *Biomineralization*; Baeuerlein, E., Ed.; Wiley-VCH: Weinheim, Germany, 2000; pp 189−206.
(24) Shimizu, K.; Morse, D. E. In *Biomineralization*; Baeuerlein, E., Ed.; Wiley-VCH: Weinheim, Germany, 2000; pp 207−220.
(25) Sahai, N. *Geochim. Cosmochim. Acta* **2004**, *68*, 227−237.
(26) Review dealing with the silicon metabolism in diatoms: Martin-Jézéquel, V.; Hildebrand, M.; Brzezinski, M. A. *J. Physiol.* **2000**, *36*, 821−840.
(27) Iler, R. K. *The Chemistry of Silica: Solubility, Polymerization, Colloid and Surface Properties, and Biochemistry*; Wiley: New York, 1978; pp 783−784.
(28) Kaufman, P. B.; Dayanandan, P.; Takeoka, Y.; Bigelow, W. C.; Jones, J. D.; Iler, R. In *Silicon and Siliceous Structures in Biological Systems*; Simpson, T. L., Volcani, B. E., Eds.; Springer-Verlag: New York, 1981; pp 442−446.
(29) Sullivan, C. W. In *Silicon Biochemistry*; Evered, D., O'Connor, M., Eds.; Wiley: Chichester, U.K., 1986; pp 70−73.
(30) Benner, K.; Klüfers, P.; Vogt, M. *Angew. Chem.* **2003**, *115*, 1088−1093; *Angew. Chem., Int. Ed.* **2003**, *42*, 1058−1062.
(31) Kinrade, S. D.; Deguns, E. W.; Gillson, A.-M.; Knight, C. T. G. *J. Chem. Soc., Dalton Trans.* **2003**, 3713−3716.

°C. ^{1}H NMR(CD_3CN): δ 0.90−0.95 (m, 18 H, CC*H*$_3$), 1.28−1.40 (m, 12 H, CC*H*$_2$CH$_3$), 1.56−1.66 (m, 12 H, NCH$_2$C*H*$_2$C), 2.49−2.82 (m, 8 H, CC*H*$_2$C(O)), 3.02−3.08 (m, 12 H, NC*H*$_2$C), 7.8 (br s, 2 H, N*H*), 11.7 (br s, 2 H, O*H*). ^{1}H NMR (CD_3OD): δ 0.96−0.99 (m, 18 H, CC*H*$_3$), 1.35−1.45 (m, 12 H, CC*H*$_2$CH$_3$), 1.64−1.70 (m, 12 H, NCH$_2$C*H*$_2$C), 2.56−3.01 (m, 8 H, CC*H*$_2$C(O)), 3.13−3.18 (m, 12 H, NC*H*$_2$C). ^{1}H NMR (D_2O): δ 0.80−0.85 (m, 18 H, CC*H*$_3$), 1.20−1.33 (m, 12 H, CC*H*$_2$CH$_3$), 1.51−1.61 (m, 12 H, NCH$_2$C*H*$_2$C), 2.60−2.77 (m, 8 H, CC*H*$_2$C(O)), 2.96−3.05 (m, 12 H, NC*H*$_2$C). ^{13}C NMR (CD_3CN): δ 13.8 (C*C*H$_3$), 20.4 (C*C*H$_2$CH$_3$), 26.1 (NCH$_2$*C*H$_2$C), 42.4 (C*C*H$_2$C(O)), 45.6 (C*C*H$_2$C(O)), 53.4 (N*C*H$_2$C), 74.1 (C$_3$*C*O), 171.2 (*C*═O), 173.5 (*C*═O), 178.6 (*C*═O).[12] ^{13}C NMR (CD_3OD): δ 14.0 (C*C*H$_3$), 20.9 (C*C*H$_2$CH$_3$), 26.7 (NCH$_2$*C*H$_2$C), 42.7 (C*C*H$_2$C(O)), 45.5 (C*C*H$_2$C(O)), 53.8 (N*C*H$_2$C), 74.8 (C$_3$*C*O), 173.1 (*C*═O), 176.7 (*C*═O), 181.5 (*C*═O). ^{13}C NMR (D_2O): δ 15.7 (C*C*H$_3$), 22.2 (C*C*H$_2$CH$_3$), 28.1 (NCH$_2$*C*H$_2$C), 44.8 (C*C*H$_2$C(O)), 47.0 (C*C*H$_2$C(O)), 55.6 (N*C*H$_2$C), 76.7 (C$_3$*C*O), 177.0 (*C*═O), 179.4 (*C*═O), 184.2 (*C*═O). Anal. Calcd for $C_{36}H_{66}GeN_2O_{14}$ (823.54): C, 52.50; H, 8.08; N, 3.40. Found: C, 52.6; H, 8.0; N, 3.4.

Crystal Structure Analysis. A suitable single crystal of **5** was obtained by crystallization from water (slow evaporation of the solvent at room temperature). The crystal was mounted in inert oil (perfluoroalkyl ether, ABCR) on a glass fiber and then transferred to the cold nitrogen gas stream of the diffractometer (Stoe IPDS diffractometer, graphite-monochromated Mo Kα radiation (λ = 0.710 73 Å)). The structure was solved by direct methods.[32] The non-hydrogen atoms were refined anisotropically.[33] A riding model was employed in the refinement of the C*H* hydrogen atoms. The O*H* and N*H* hydrogen atoms were localized in difference Fourier syntheses and refined freely. In addition to the Supporting Information described at the end of this paper, crystallographic data (excluding structure factors) for the structure reported in this paper have been deposited with the Cambridge Crystallographic Data Centre as supplementary publication no. CCDC-249757 (**5**). Copies of the data can be obtained free of charge on application to CCDC, 12 Union Road, Cambridge CB2 1EZ, U.K. (fax, (+44)-1223/336033; e-mail, deposit@ccdc.cam.ac.uk).

SANS Experiments. The SANS experiments were performed at the diffractometers for small-angle scattering KWS1 and KWS2 at the FRJ-2 of the research center in Jülich, Germany (for more detailed information of the experimental equipment, see ref 34). The experiments were performed at three detector-to-sample positions between 2 and 20 m with neutrons of 7 Å wavelength and a wavelength distribution of $\Delta\lambda/\lambda$ = 0.2. This instrumental setting allowed us to measure in a Q range between 0.002 and 0.2 Å^{-1}. The data from all samples including solvents were analyzed by standard procedures considering background and sensitivity of the single detector channels. The absolute calibration was achieved by a secondary standard sample. Finally, the scattering of the solvent as well as the incoherent scattering of the silica particles after being weighted with the molecular volume fraction was subtracted from $d\Sigma/d\Omega(Q)$. The incoherent scattering of the silica particles had to be evaluated.[14]

Acknowledgment. We thank the Deutsche Forschungsgemeinschaft (priority program "Principles of Biomineralization") and the Fonds der Chemischen Industrie for financial support.

Supporting Information Available: Tables of atomic coordinates and equivalent isotropic displacement parameters, anisotropic displacement parameters, experimental details of the X-ray diffraction studies, and bond lengths and angles for **5** (cif format); checkCIF/PLATON report (pdf). This material is available free of charge via the Internet at http://pubs.acs.org.

IC048748W

(32) (a) Sheldrick, G. M. *SHELXS-97*; University of Göttingen: Göttingen, Germany, 1997. (b) Sheldrick, G. M. *Acta Crystallogr., Sect. A* **1990**, *46*, 467−473.

(33) Sheldrick, G. M. *SHELXL-97*; University of Göttingen: Göttingen, Germany, 1997.

(34) Web-site: www.neutronscattering.de.